Sub-Kelvin hysteresis of the dilanthanide single-molecule magnet $Tb_2ScN@C_{80}$

Aram Kostanyan,[1] Rasmus Westerström,[2] David Kunhardt,[3] Bernd Büchner,[3] Alexey A. Popov,[3] and Thomas Greber[1,*]

[1]*Physik-Institut, Universität Zürich, Winterthurerstrasse 190, CH-8057 Zürich, Switzerland*

[2]*Division of Synchrotron Radiation Research, Institute of Physics, Lund University, SE-221 00 Lund, Sweden*

[3]*Leibniz Institute for Solid State and Materials Research, Dresden, D-01069 Dresden, Germany*

(Received 6 September 2019; revised manuscript received 30 March 2020; accepted 1 April 2020; published 27 April 2020)

Magnetic hysteresis is a direct manifestation of nonequilibrium physics that has to be understood if a system is to be used for information storage and processing. The dilanthanide endofullerene $Tb_2ScN@C_{80}$ is shown to be a single-molecule magnet with a remanence time on the order of 100 s at 400 mK. Three different temperature-dependent relaxation barriers are discerned. The lowest 1 K barrier is assigned to intermolecular dipole-dipole interaction, the 10 K barrier to intramolecular exchange and dipolar coupling, and the 50 K barrier to molecular vibrations as was observed for $Dy_2ScN@C_{80}$. The 4 orders of magnitude difference in the prefactor between the Tb and the Dy compound in the decay process across the 10 K barrier is assigned to the lack of Kramers protection in Tb^{3+}. The sub-Kelvin hysteresis follows changes in the magnetization at level crossings of the four possible Tb_2 ground-state configurations. Comparison to a hysteresis model, with magnetic relaxation at level crossings only, reveals cooperative action between nearby molecules.

DOI: 10.1103/PhysRevB.101.134429

I. INTRODUCTION

Single-molecule magnets realize bistable spin configurations with lifetimes on the order of seconds or longer [1]. While their magnetization may change via thermal fluctuations, there are as well temperature-independent quantum flip mechanisms due to the tunneling of the magnetization [2,3]. For the identification and use of quantum effects, experiments have to be performed at sub-Kelvin temperatures, where temperature-induced switching between different magnetic states is minimal.

An important horizon in the research on single-molecule magnets was reached by the discovery of hysteresis in double-decker phthalocyanine complexes (Pc_2Ln), where one lanthanide ion is sandwiched by two organic moieties [4]. With the terbium Pc_2Ln derivative it was shown later that the four nuclear spin levels of the terbium atom may be addressed and manipulated in a molecular break junction [5]. Currently dysprosium ions in optimized molecular ligand fields display hysteresis of 60 K [6] and even above liquid nitrogen temperatures [7]. After having reached the fundamental limit of single-ion magnetism the question of how two magnetic ions interact is an obvious continuation of exploration. For the case of two holmium atoms on magnesium oxide at a separation distance of 1.2 nm the bistability of the individual Ho atoms appeared not to be influenced by the magnetic neighbourhood and they could be addressed as classical bits [8]. In molecules containing two magnetic ions at closer distance, the exchange and dipolar interaction may lead to stabilization of a specific spin configuration [9–14]. In order to examine the coupling between magnetic moments it is essential to have a stable, atomically precise environment of the spin system with a geometry where the interaction is not negligible. Endohedral single-molecule magnets meet these requirements since it is possible to place two lanthanides with distances below 0.4 nm in a C_{80} cage [15]. Before single single-molecule magnet experiments like in Ref. [5] are performed, it is desirable to investigate ensembles of single-molecule magnets. This allows an accurate determination of the magnetic lifetimes and a faster screening for the "ideal" molecule. Here we report on the magnetization of $Tb_2ScN@C_{80}$ ensembles. The pseudospin model of Westerström *et al.* [11] may be successfully applied to the description of the electronic ground state, though we find quantitative differences to $Dy_2ScN@C_{80}$. This is reflected in the hysteresis, i.e., the memory of the magnetization history. Hysteresis occurs whenever the magnetization in a field scan does not follow the ground state. The hysteresis depends on the lifetime of a given magnetization for a given applied field. This explains why a quantitative prediction of the hysteresis curve for single-molecule magnets is more involved than the description of the magnetization at thermal equilibrium. Steps and kinks in hysteresis are often associated with level crossings [2]. Since the level crossings depend on the applied field vector and the anisotropy axes, single-crystal and single-molecule experiments at lowest temperatures display the sharpest steps. Magnetization hysteresis of rare-earth ions substituted in $LiYF_4$ and in molecule crystals has been investigated at sub-Kelvin temperatures before [12,16,17]. In the present paper we report sharp steps in the hysteresis for an anisotropic $Tb_2ScN@C_{80}$ powder sample. These steps are related to the crossings of quantum levels with different spin configurations that occur in a narrow external magnetic field window. The simplicity of the spin configuration in the present

*greber@physik.uzh.ch

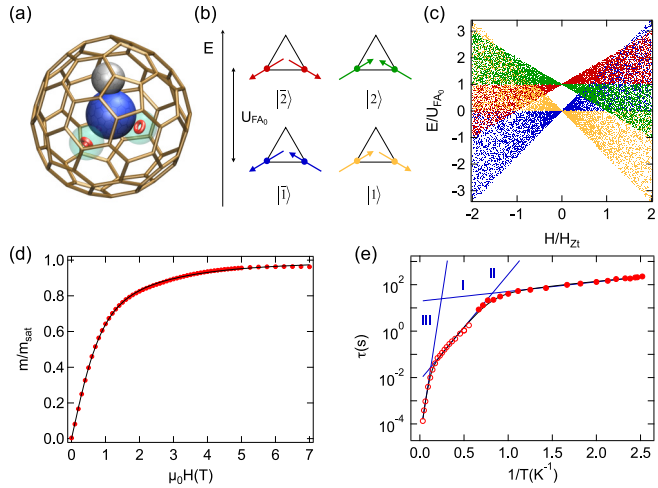

FIG. 1. (a) Model of the dilanthanide single-molecule magnet $Tb_2ScN@C_{80}$. The sizes of the endohedral ions are mimicked with their ion radii. In the center of the Tb^{3+} ions (turquoise) the $4f$ ($J_z = 6$) orbitals are depicted in red [18,19]. (b) Zero-field ground states. The magnetic moments μ of the two Tb ions sit on an equilateral triangle and point into the center or away from it. Two doublets form, where $|\bar{1}\rangle$ (blue) and $|1\rangle$ (yellow) have ferromagnetic coupling, while $|\bar{2}\rangle$ (red) and $|2\rangle$ (green) are antiferromagnetically coupled. In zero field the energy difference between the two doublets is U_{FA_0}. (c) Energies for the four ground states of 10 000 molecules oriented randomly with respect to the axis of the applied H field. The color coding is adopted from panel (b). No level crossings between the two doublets are expected for $|H| < U_{FA_0}/2\mu_0\mu$ [20]. (d) Magnetization curve at 6 K and fit of the pseudospin model (black line) after diamagnetic background subtraction resulting in $\mu = 8.8\ \mu_B$ and $U_{FA_0}/k_B = 9.4$ K. (e) Arrhenius plot of the magnetization lifetimes. Solid symbols are DC measurements with the ^{3}He cryostat, and open symbols are AC susceptibility measurements. The black curve is the sum of three Arrhenius processes: I, II, and III (the slopes of the blue lines represent the individual process barriers).

molecule allows the modeling of the hysteresis with level crossings only and a quantitative comparison to the observed hysteresis curve.

II. EXPERIMENTAL

$Tb_2ScN@C_{80}$ [see Fig. 1(a)] endofullerenes were produced by arc-discharge synthesis using the corresponding metals [21]. For the magnetization measurements the toluene solution of $Tb_2ScN@C_80$ was drop-cast into a polypropylene sample holder resulting in a visible black powder residue. From the saturation magnetization of $2.98 \times 10^{17}\mu_B$ and an average molecular moment of 9 μ_B, an ensemble of 3.3×10^{16} molecules or 73.5 μg is inferred. The magnetization was measured in a Quantum Design MPMS3 vibrating sample magnetometer (VSM) with a ^{3}He cryostat. AC magnetization measurements were performed in the temperature range between 1.8 and 30 K at zero (<0.5 mT) DC magnetic field with a driving AC field amplitude of 1 mT up to 10 Hz and 0.25 mT between 10 Hz and 1 kHz.

III. RESULTS

A. Ground state

Figure 1(b) shows the model of the ground state of $Tb_2ScN@C_{80}$ in zero external magnetic field. The two paramagnetic Tb^{3+} ions in the Tb_2ScN endohedral unit constitute the molecular magnetism. Some degeneracies of the eight $4f$ electrons in the spherical $^7F_6$ Hund manifolds are lifted in the ligand field that is dominated by the central N^{3-} ion. As for Dy [11] and Ho [22], the maximum projections of J assume the ground states, which are in the case of terbium the $J_z = \pm 6$ levels with a nominal magnetic moment of $\mu = \pm 9\ \mu_B$ along the Tb-N axes. The anisotropy is high and other J_z states may be neglected since they have energies that are much higher than the thermal energies in the present experiments [23]. Below 50 K, the molecule orientation is frozen, and the ground states of the individual molecules are determined by the orientation of the external magnetic field with respect to that of the magnetic moments on the two Tb atoms [24,25]. For a given molecular orientation this yields 2^2 possible ground-state configurations that split into two time-reversal symmetric doublets spanning the Hilbert space. The states $|1\rangle$ and $|\bar{1}\rangle$ are ferromagnetically coupled and the states $|2\rangle$ and $|\bar{2}\rangle$ are antiferromagnetically coupled where the energy difference U_{FA_0} is reflected in the magnetization curves. In $Tb_2ScN@C_{80}$, $|1\rangle$ and $|\bar{1}\rangle$ in zero field have energy lower than that of $|2\rangle$ and $|\bar{2}\rangle$, as was found for $Dy_2ScN@C_{80}$ [11], while, e.g., in $Dy_2O@C_{82}$ antiferromagnetic coupling is favored [14]. For Tb ions sitting on two vertices of an equilateral triangle, the total magnetic moments of $|1\rangle$ and $|\bar{1}\rangle$ and of $|2\rangle$ and $|\bar{2}\rangle$ are orthogonal and $\pm\sqrt{3}\mu$ for the ferromagnetic doublet and $\pm\mu$ for the antiferromagnetic doublet. The energy difference between the two doublets has exchange and dipolar components and in an external magnetic field the degeneracies of the doublets are lifted by the corresponding Zeeman splitting. The magnetism is noncollinear, i.e., the magnetic moments are not aligned to the external field but to the molecular coordinates that determine the anisotropy axes. In zero-field-cooled powder samples, there is no preferential molecular orientation and the distribution of the Tb-N axes is isotropic [25]. In Fig. 1(c) the energies of an ensemble of isotropically distributed molecules in different external magnetic fields are displayed. The energy and field scales in Fig. 1(c) are U_{FA_0}, and the Zeeman threshold field above which antiferro states with an according orientation in the field may get the lowest energy $H_{Zt} \equiv U_{FA_0}/\mu_0\mu$.

In Fig. 1(d) the equilibrium magnetization for $Tb_2ScN@C_{80}$ at 6 K is shown with a corresponding fit of the pseudospin model. The fit yields a Tb magnetic moment μ of $8.8 \pm 0.4\ \mu_B$ and an exchange and dipolar barrier U_{FA_0}/k_B of 9.4 ± 1.5 K. These parameters determine the Zeeman threshold field $\mu_0 H_{Zt} = 1.6 \pm 0.3$ T. It is known that U_{FA_0} is also reflected in nonequilibrium data as it is the decay time to reach equilibrium [11]. Figure 1(e) displays the zero-field magnetization lifetimes of $Tb_2ScN@C_{80}$ in an Arrhenius plot in the temperature range between 0.4 and 30 K [20]. From the fit, three different decay processes with barriers Δ_{eff}^i and prefactors $\tau_{0,i}$ as listed in Table I are inferred. Process II is identified as the decay that is mediated via the excitation across U_{FA_0}, and Δ_{eff}^{II} of 10.5 K is comparable to

TABLE I. Fit parameters of three Arrhenius barriers for the temperature dependence of the zero-field magnetization relaxation times τ of $Tb_2ScN@C_{80}$ in Fig. 1(e): $\tau^{-1} = \sum_{i=\mathrm{I}}^{\mathrm{III}} \tau_{0,i}^{-1} \exp(-\Delta_{\mathrm{eff}}^{i}/k_B T)$.

Process	τ_0 (s)	$\Delta_{\mathrm{eff}}/k_B$ (K)
I	$(2.0 \pm 0.3) \times 10^{1}$	1 ± 0.1
II	$(7.7 \pm 0.1) \times 10^{-3}$	10.5 ± 0.3
III	$(2.6 \pm 0.5) \times 10^{-5}$	56.4 ± 3.0

that of $Dy_2ScN@C_{80}$ (8.5 K) [11]. On the other hand, the prefactor of $Tb_2ScN@C_{80}$ is 4 orders of magnitude smaller. This must be related to the even electron number in Tb $4f^8$ and the odd electron number in Dy $4f^9$, which is a Kramers ion. Apparently, the two ground states $|1\rangle$ and $|\bar{1}\rangle$ may better hybridize in the case of $Tb_2ScN@C_{80}$.

The 1 K barrier cannot be explained within the ground-state picture in Fig. 1(b). Also, it appears larger than the energy scale of the hyperfine interaction in ^{159}Tb where the four nuclear spin levels are separated by less than 0.5 k_B K [26]. It rather points to intermolecular dipolar interactions as they were, e.g., proposed to explain a 1.2 K transition in an Fe_{19} nanodisk system [27]. For the present case of close-packed $Tb_2ScN@C_{80}$ with randomly oriented endohedral units, we get from Monte Carlo simulations equilibrium dipolar interaction energy distributions with a full width at half maximum of 0.84 k_B K [20], which is close to the observed barrier $\Delta_{\mathrm{eff}}^{\mathrm{I}}$ of 1 k_B K. The barrier of the fastest process, process III, is similar to one in $Dy_2ScN@C_{80}$ [11] and likely involves molecular-vibration-assisted transitions.

B. Hysteresis model

In the following, a theory for hysteresis that allows for changes in magnetization at $4f$ electron level crossings only is outlined. Figure 2 shows the Zeeman energies for two molecular orientations relative to the external field of the $|1\rangle$, $|\bar{1}\rangle$ and the $|2\rangle$, $|\bar{2}\rangle$ doublets and their corresponding contribution to the magnetization. The majority group with ferromagnetic ground states at all fields $|1\rangle$ or $|\bar{1}\rangle$ is called the F branch and one example is depicted in Fig. 2(a). The minority group with antiferromagnetic ground states in fields above H_{Zt} or below $-H_{\mathrm{Zt}}$, $|2\rangle$ or $|\bar{2}\rangle$, is called the A branch and is represented in Fig. 2(b). At level crossings the magnetization of the given molecules may flip between two values without cost or release of energy. This is visualized in the bottom panels, where the different effective magnetic moments $\mu_i = dE_i/d\mu_0 H$ and their occupancies are displayed. Both branches have six level crossings, though the topology, or crossing sequence, is different for the F branch and the A branch. We distinguish two zero-field crossings, $|\bar{1}\rangle \leftrightarrow |1\rangle$ and $|\bar{2}\rangle \leftrightarrow |2\rangle$, which involve the simultaneous flip of the two pseudospins that constitute the state, and four nonzero-field crossings, $|\bar{2}\rangle \leftrightarrow |\bar{1}\rangle$, $|\bar{2}\rangle \leftrightarrow |1\rangle$, $|\bar{1}\rangle \leftrightarrow |2\rangle$, and $|1\rangle \leftrightarrow |2\rangle$, which involve one spin flip only. For scenarios where the change in magnetization occurs at

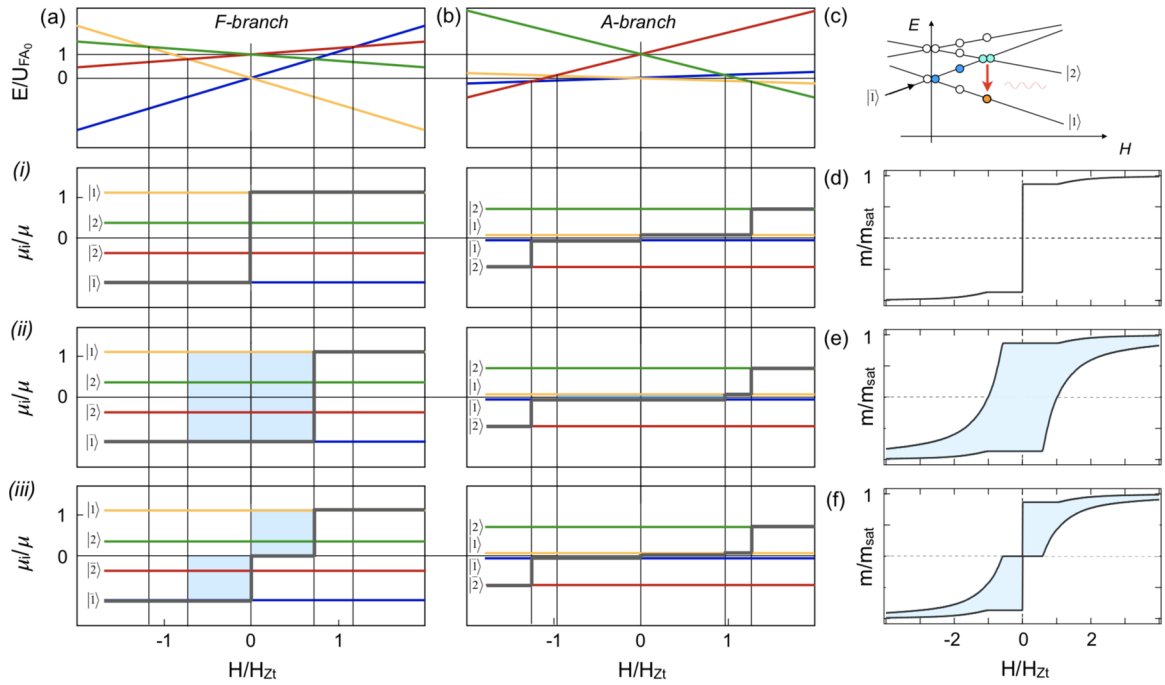

FIG. 2. The six different level crossings within the four ground states $|1\rangle$, $|\bar{1}\rangle$, $|2\rangle$, and $|\bar{2}\rangle$ (yellow, blue, green, and red) in a Zeeman E vs H diagram and corresponding magnetization curves. (a) Example of an F-branch orientation with ferromagnetic ground states. (b) Example of an A-branch orientation with antiferromagnetic ground states in large fields. The bottom panels show the magnetization as expected for the different scenarios (i), (ii), and (iii) (for details see text). (c) Crossing that reassumes nonadiabatically the ground state with energy dissipation for a field scan from negative to positive external fields. Upon crossing of the $|\bar{1}\rangle$ state and the $|2\rangle$ state one spin may flip without cost of energy, and the second spin may flip under the release of energy into the $|1\rangle$ state. (d)–(f) Magnetization curves of the sum of randomly oriented molecules for the three scenarios. While the adiabatic scenario (i) displays no hysteresis, the two scenarios with nonadiabatic jumps in the magnetization do.

level crossings only, we construct the magnetization curves of the ensemble from the sum of the projected (effective) magnetic moments of all molecular orientations. If the magnetization in a field-scan were to follow the lowest energy, no hysteresis would be expected. In order to observe hysteresis we rely on crossings where the system prevails in its magnetization state and leaves the lowest-energy curve and where it jumps in subsequent crossings nonadiabatically to the lowest energy. In Figs. 2(a) and 2(b) the magnetization is shown for three scenarios and the F branch and the A branch, where the field scan starts at saturation in large negative fields, i.e., $|\bar{1}\rangle$ or $|\bar{2}\rangle$: (i) lowest energy, (ii) crossing at zero field and nonadiabatic relaxation upon the single flip crossing $|\bar{1}\rangle \rightarrow |2\rangle \searrow |1\rangle$, and (iii) equilibration at zero field into 50% $|1\rangle$ and 50% $|\bar{1}\rangle$ and nonadiabatic relaxation at the single flip crossing $|\bar{1}\rangle \rightarrow |2\rangle \searrow |1\rangle$ as shown in Fig. 2(c). The magnetization in the purely adiabatic scenario (i) in Fig. 2(d) displays no hysteresis, but the deviation from the step function discerns the influence of the A branch and the "gap" between $\pm H_{Zt}$, where in the ground state no single flip crossings occur. For the two scenarios with nonadiabatic relaxations in Figs. 2(e) and 2(f), the state distribution depends on the field scan direction, and correspondingly hysteresis turns up. Importantly, we see that $|\bar{1}\rangle \rightarrow |2\rangle \searrow |1\rangle$ crossings of excited states may occur in the ground state crossing gap for $H > H_{Zt}/2$ where these transitions sharply peak above $H_{Zt}/2$ [20]. This theory provides an upper limit for the deviation of the magnetization from the equilibrium and is a benchmark for the characterization of the hysteresis of dilanthanide single-molecule magnets. It also allows predictions for single-molecule and single-crystal experiments.

C. Comparison between experiment and theory

The three scenarios in Fig. 2 may be compared to sub-Kelvin magnetization data. Figure 3 shows the magnetization curve for $Tb_2ScN@C_{80}$ at 390 mK with a field scan rate of 3.3 mT/s. Starting at zero field the magnetization jumps within 60 s to 20% of the saturation magnetization, where it remains constant before it continues to rise at 0.75 T external field. This can be understood within the ground-state picture of Fig. 1(b). Near-zero-field fluctuations between $|1\rangle$ and $|\bar{1}\rangle$ states prevail and the rise of the external field increases the magnetization. Between $\mu_0 H$ of 0.2 and 0.7 T the fluctuations are suppressed due to Zeeman energies exceeding $k_B T$ and the magnetization appears to be frozen. At $\mu_0 H = 0.75$ T the magnetization rises again. This field corresponds to $\mu_0 H_{Zt}/2$ and is a confirmation that $|\bar{1}\rangle \rightarrow |2\rangle \searrow |1\rangle$ transitions drive the increase of magnetization towards saturation. If the field scan direction is inverted the system remains in a high magnetization state down to zero field where equilibration is most effective. The observed hysteresis compares best with scenario (iii), where we observe a kink in the lower branch of the magnetization curve at half the threshold field H_{Zt} and strong demagnetization at zero field. Still, the measured hysteresis indicates less magnetization hysteresis than would be expected if level crossings only would cause changes in the magnetization of the sample. In line with the 1 K barrier,

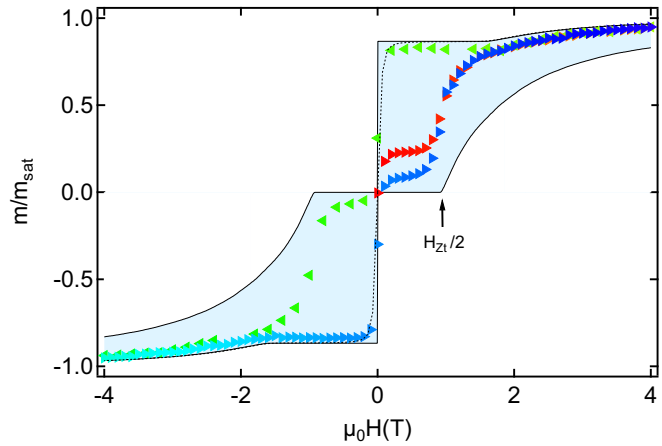

FIG. 3. Magnetization loop of $Tb_2ScN@C_{80}$ recorded at 390 mK with a field scan rate of ± 3.3 mT/s. The red-green-blue color code of the experimental data represents the time during the field scan that starts with the virgin curve at $H = 0$ (red). The triangles indicate the positive ($\triangleright$) and negative ($\triangleleft$) field scan rates. The light blue area represents the zero-temperature hysteresis of scenario (iii). $H_{Zt}/2$ is the magnetic field at which the onset of nonadiabatic decay of magnetization is expected. The dotted line is the theoretical equilibrium magnetization curve at 390 mK.

this confirms that at 400 mK other processes contribute to the decay of the magnetization toward thermal equilibrium. The energy and the angular momentum that are released during magnetization reversal of a molecule have to be dissipated and may trigger cooperative effects, like the flipping of magnetic moments on neighbor molecules, as they are found in spin glasses [28].

In Fig. 4 the rate $\frac{dm}{d\mu_0 H}$ with which the magnetization approaches the saturation magnetization is shown for

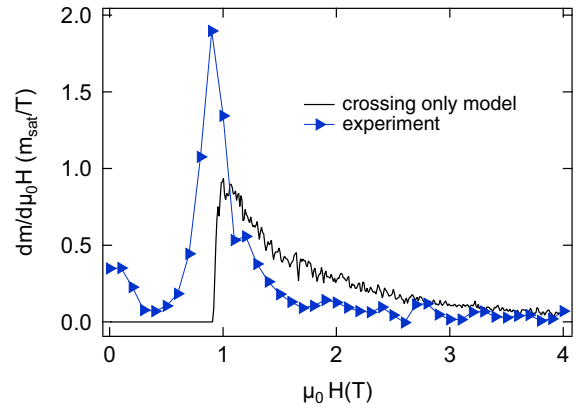

FIG. 4. Rate $\frac{dm}{d\mu_0 H}$ with which the magnetization of an ensemble of molecules approaches the saturation magnetization as a function of the external magnetic field $\mu_o H$. The black line is the rate as expected from the hysteresis with the change of magnetization upon crossing model with the Zeeman threshold field for $Tb_2ScN@C_{80}$ of $\mu_0 H_{Zt} = 1.6$ T, while the blue triangles are the experimental values for the corresponding hysteresis branch at 390 mK for a field sweep rate β of 3.3 mK s^{-1}.

the experiment and the hysteresis with the change of magnetization upon crossing only. For $Tb_2ScN@C_{80}$, both theoretical and experimental rates peak at a field of about 1 T. The experimental rate near zero field is not zero due to tunneling of the magnetization, while the main peak at 1 T is sharper than the theoretical counterpart. For higher fields the experimental rate drops below the theoretical rate, which must be due to the flip of magnetization of individual molecules before their nominal level crossing. The dissipation power P per molecule is written as

$$P = \frac{dE}{dt} = \beta\mu_0 H \frac{dm}{d\mu_0 H}, \tag{1}$$

where β is the field sweep rate and H is the external magnetic field. The experimental peak corresponds to a power of dissipated energy of about 1.6 μW for the sample of $N = 2 \times 10^{17}$ $Tb_2ScN@C_{80}$ molecules. Part of the related energy and angular momentum may be transferred to the nearby magnetic moments and trigger a cooperative, avalanche-like decay.

IV. CONCLUSIONS

In conclusion $Tb_2ScN@C_{80}$ is shown to be a single-molecule magnet with a ground-state configuration that causes a sub-Kelvin hysteresis with kinks, which coincide with adiabatic zero-field crossings and nonadiabatic nonzero-field crossings at a characteristic external magnetic field. The findings can be translated to any single-molecule magnet with two spin centers.

ACKNOWLEDGMENTS

Financial support from the Swiss National Science Foundation (Projects No. 200021L_147201 and No. 206021_-150784), the European Unions Horizon 2020 Research and Innovation Program, the European Research Council (Grant No. 648295 to A.A.P.), the Deutsche Forschungsgemeinschaft (DFG Projects PO 1602/4-1 and PO 1602/5-1), and the Swedish Research Council (Grant No. 301 2015-00455) and Sklodowska Curie Actions co-founding project INCA 600398 is acknowledged. We thank Ari P. Seitsonen for the artwork in Fig. 1.

[1] D. Gatteschi, R. Sessoli, and J. Villain, *Molecular Nanomagnets* (Oxford University, Oxford, 2006).

[2] L. Thomas, F. Lionti, R. Ballou, D. Gatteschi, R. Sessoli, and B. Barbara, Macroscopic quantum tunneling of magnetization in a single crystal of nanomagnets, Nature (London) **383**, 145 (1996).

[3] Z. Zhu, M. Guo, X. L. Li, and J. Tang, Molecular magnetism of lanthanide: Advances and perspectives, Coord. Chem. Rev. **378**, 350 (2019).

[4] N. Ishikawa, M. Sugita, T. Ishikawa, S. Koshihara, and Y. Kaizu, Lanthanide double-decker complexes functioning as magnets at the single-molecular level, J. Am. Chem. Soc. **125**, 8694 (2003).

[5] R. Vincent, S. Klyatskaya, M. Ruben, W. Wernsdorfer, and F. Balestro, Electronic read-out of a single nuclear spin using a molecular spin transistor, Nature (London) **488**, 357 (2012).

[6] C. A. P. Goodwin, F. Ortu, D. Reta, N. F. Chilton, and D. P. Mills, Molecular magnetic hysteresis at 60 Kelvin in dysprosocenium, Nature (London) **548**, 439 (2017).

[7] F. S. Guo, B. M. Day, Y. C. Chen, M. L. Tong, A. Mansikkamaki, and R. A. Layfield, Magnetic hysteresis up to 80 Kelvin in a dysprosium metallocene single-molecule magnet, Science **362**, 1400 (2018).

[8] F. D. Natterer, K. Yang, W. Paul, P. Willke, T. Choi, T. Greber, A. J. Heinrich, and C. P. Lutz, Reading and writing single-atom magnets, Nature (London) **543**, 226 (2017).

[9] J. D. Rinehart, M. Fang, W. J. Evans, and J. R. Long, Strong exchange and magnetic blocking in N-2(3-)-radical-bridged lanthanide complexes, Nat. Chem. **3**, 538 (2011).

[10] Y. N. Guo, G. F. Xu, W. Wernsdorfer, L. Ungur, Y. Guo, J. Tang, H. J. Zhang, L. F. Chibotaru, and A. K. Powell, Strong axiality and Ising exchange interaction suppress zero-field tunneling of magnetization of an asymmetric Dy_2 single-molecule magnet, J. Am. Chem. Soc. **133**, 11948 (2011).

[11] R. Westerström, J. Dreiser, C. Piamonteze, M. Muntwiler, S. Weyeneth, K. Krämer, S. X. Liu, S. Decurtins, A. Popov, S. Yang, L. Dunsch, and T. Greber, Tunneling, remanence, and frustration in dysprosium-based endohedral single-molecule magnets, Phys. Rev. B **89**, 060406(R) (2014).

[12] T. Morita, M. Damjanovic, K. Katoh, Y. Kitagawa, N. Yasuda, Y. Lan, W. Wernsdorfer, B. K. Breedlove, M. Enders, and M. Yamashita, Comparison of the magnetic anisotropy and spin relaxation phenomenon of dinuclear terbium(III) phthalocyaninato single-molecule magnets using the geometric spin arrangement, J. Am. Chem. Soc. **140**, 2995 (2018).

[13] F. Liu, G. Velkos, D. S. Krylov, L. Spree, M. Zalibera, R. Ray, N. A. Samoylova, C. H. Chen, M. Rosenkranz, S. Schiemenz, F. Ziegs, K. Nenkov, A. Kostanyan, T. Greber, A. U. B. Wolter, M. Richter, B. Büchner, S. M. Avdoshenko, and A. A. Popov, Air-stable redox-active nanomagnets with lanthanide spins radical-bridged by a metal-metal bond, Nat. Commun. **10**, 571 (2019).

[14] W. Yang, G. Velkos, F. Liu, S. M. Sudarkova, Y. Wang, J. Zhuang, H. Zhang, X. Li, X. Zhang, B. Büchner, S. M. Avdoshenko, A. A. Popov, and N. Chen, Single molecule magnetism with strong magnetic anisotropy and enhanced Dy$\cdots$Dy coupling in three isomers of Dy-oxide cluster-fullerene $Dy_2O@C_{82}$, Adv. Sci. **6**, 1901352 (2019).

[15] A. A. Popov, S. Yang, and L. Dunsch, Endohedral fullerenes, Chem. Rev. **113**, 5989 (2013).

[16] R. Giraud, W. Wernsdorfer, A. Tkachuk, D. Mailly, and B. Barbara, Nuclear Spin Driven Quantum Relaxation in $LiY_{0.998}Ho_{0.002}F_4$, Phys. Rev. Lett. **87**, 057203 (2001).

[17] R. J. Blagg, L. Ungur, F. Tuna, J. Speak, P. Comar, D. Collison, W. Wernsdorfer, E. J. L. McInnes, L. F. Chibotaru, and R. E. P. Winpenny, Magnetic relaxation pathways in lanthanide single-molecule magnets, Nat. Chem. **5**, 673 (2013).

[18] J. Sievers, Asphericity of $4f$-shells in their Hund's rule ground states, Z. Phys. B **45**, 289 (1982).

[19] T. Greber, A. P. Seitsonen, A. Hemmi, J. Dreiser, R. Stania, F. Matsui, M. Muntwiler, A. A. Popov, and R. Westerstrom, Circular dichroism and angular deviation in x-ray absorption spectra of $Dy_2ScN@C_{80}$ single-molecule magnets on h-BN/Rh(111), Phys. Rev. Mater. **3**, 014409 (2019).

[20] See Supplemental Material at http://link.aps.org/supplemental/10.1103/PhysRevB.101.134429 for ^{3}He magnetisation lifetime measurements; AC magnetisation lifetime measurements; Modelling intermolecular dipole-dipole interaction; Level crossing densities.

[21] Y. Zhang, D. Krylov, M. Rosenkranz, S. Schiemenz, and A. A. Popov, Magnetic anisotropy of endohedral lanthanide ions: Paramagnetic NMR study of $MSc_2N@C_{80}$-I_h with M running through the whole 4f row, Chem. Sci. **6**, 2328 (2015).

[22] J. Dreiser, R. Westerstrom, Y. Zhang, A. A. Popov, L. Dunsch, K. Kraemer, S. X. Liu, S. Decurtins, and T. Greber, The metallofullerene field-induced single-ion magnet $HoSc_2N@C_{80}$, Chem. - Eur. J. **20**, 13536 (2014).

[23] F. Cimpoesu, N. Dragoe, H. Ramanantoanina, W. Urland, and C. Daul, The theoretical account of the ligand field bonding regime and magnetic anisotropy in the $DySc_2N@C_{80}$ single ion magnet endohedral fullerene, Phys. Chem. Chem. Phys. **16**, 11337 (2014).

[24] W. Fu, X. Wang, H. Azuremendi, J. Zhang, and H. C. Dorn, ^{14}N and ^{45}Sc NMR study of trimetallic nitride cluster $(M_3N)^{6+}$ dynamics inside a icosahedral C_{80} cage, Chem. Commun. **47**, 3858 (2011).

[25] A. Kostanyan, R. Westerstrom, Y. Zhang, D. Kunhardt, R. Stania, B. Büchner, A. A. Popov, and T. Greber, Switching Molecular Conformation with the Torque on a Single Magnetic Moment, Phys. Rev. Lett. **119**, 237202 (2017).

[26] S. Thiele, R. Vincent, M. Holzmann, S. Klyatskaya, M. Ruben, F. Balestro, and W. Wernsdorfer, Electrical Readout of Individual Nuclear Spin Trajectories in a Single-Molecule Magnet Spin Transistor, Phys. Rev. Lett. **111**, 037203 (2013).

[27] F. L. Pratt, E. Micotti, P. Carretta, A. Lascialfari, P. Arosio, T. Lancaster, S. J. Blundell, and A. K. Powell, Dipolar ordering in a molecular nanomagnet detected using muon spin relaxation, Phys. Rev. B **89**, 144420 (2014).

[28] K. Binder and A. P. Young, Spin-glasses—Experimental facts, theoretical concepts, and open questions, Rev. Mod. Phys. **58**, 801 (1986).